Scanning Tunneling Microscopy of Mixed Valence Dinuclear Organometallic Cations and Counterions on Au(111)

ARTICLE *in* JOURNAL OF PHYSICAL CHEMISTRY LETTERS · DECEMBER 2009

Impact Factor: 7.46 · DOI: 10.1021/jz900197a

THE JOURNAL OF PHYSICAL CHEMISTRY Letters

pubs.acs.org/JPCL

Scanning Tunneling Microscopy of Mixed Valence Dinuclear Organometallic Cations and Counterions on Au(111)

Song Guo[†] and S. Alex Kandel*

Department of Chemistry and Biochemistry, University of Notre Dame, Notre Dame, Indiana 46556

ABSTRACT Single-molecule electronic components are potential building blocks for next-generation electronic devices. One architecture for such devices is quantum dot cellular automata (QCA), in which binary information is encoded in the charge configuration of a single cell and transferred by electric coupling between neighboring cells. A single mixed-valence molecule with two oxidation−reduction centers can serve as a QCA cell, and ensemble measurements have shown that such molecules may have the desired electronic properties. Scanning tunneling microscopy (STM) is used to image dinuclear metal complexes, *trans*-[Cl-(dppe)$_2$Ru(C≡C)$_6$Ru(dppe)$_2$Cl] (**Ru2**) on Au(111) at 77 K. Oxidation to **Ru2**$^+$[PF$_6$]$^-$ creates an unbalanced charge that localizes on one end group of the otherwise symmetric **Ru2** molecule. This electronic asymmetry appears in STM images, which also resolve the associated [PF$_6$]$^-$ counterions. Comparison of **Ru2** and **Ru2**$^+$ monolayers show that Coulomb interactions create long-range ordering of **Ru2**$^+$ electronic charge. This is a requirement for functionality in a QCA device.

SECTION Surfaces, Interfaces, Catalysis

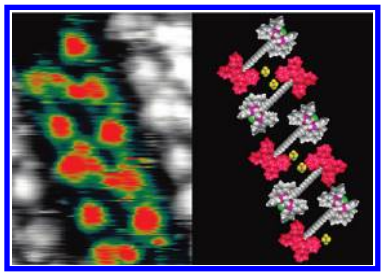

Single-molecule electronic components have been investigated as the building blocks for next-generation electronic devices.[1−12] One proposed architecture for such devices is based upon quantum dot cellular automata (QCA), in which binary information is encoded in the charge configuration of a single cell and transferred by electric coupling between neighboring QCA cells.[13−17] Implementation of QCA at the molecular level requires mixed-valence molecules with two or more oxidation−reduction centers, and such molecules have been shown to have the desired electronic properties using ensemble measurement techniques.[18,19] For the fabrication of devices, it is imperative to understand the changes in charge configuration that result when an electron tunnels between redox sites in a single molecule on a surface.[20] In our work, we present the scanning tunneling microscopy (STM) studies of dinuclear metal complexes, *trans*-[Cl(dppe)$_2$Ru(C≡C)$_6$Ru(dppe)$_2$Cl] (abbreviated as **Ru2**, dppe ≅ diphenylphosphinoethane) on Au(111) at cryogenic temperature. Close-packed **Ru2** molecules form monolayers with ordered stripes on Au(111) at 77 K. **Ru2**$^+$[PF$_6$]$^-$, the oxidation product of **Ru2**, has an extra charge which can tunnel between two metal-centered end groups. **Ru2**$^+$ cations are imaged also as a pair of dots on Au(111) and form similar striped monolayers, except that the two dots appear to have different contrast in STM images due to the extra charge localized in one end group. [PF$_6$]$^-$ anions are observed as a small dot resting next to the positively charged ends of **Ru2**$^+$ cations.

The dinuclear metal complex **Ru2** is composed of two Ru-centered phenylphosphine groups connected by a linear hexa-alkyne-bond linker, as shown in Figure 1A. While **Ru2** is a neutral dinuclear complex with both Ru metal atoms in the +2 valence state, oxidation to **Ru2**$^+$ results in a mixed-valence +2/+3 molecule with an odd electron that can tunnel between the Ru centers through the conjugated 12-carbon linker. **Ru2**$^+$ is a condidate for a two-charge-container QCA cell.[13,19,21]

Figure 1B shows a STM image of an isolated **Ru2** molecule on Au(111) at room temperature. We have characterized isolated Ru2 molecules in previous publications[22,23] and found that each pair of bright features is associated with a single **Ru2** molecule, with each bright feature corresponding to one of the Ru-based metal−ligand complexes. The two bright features appear symmetric in STM images, as would be expected from the chemical structure shown in Figure 1C.

When imaging at 77 K, we observe that **Ru2** molecules aggregate into close-packed islands on Au(111), as shown in Figure 2A. **Ru2** molecules line up side-by-side into rows, and multiple molecular rows with an inter-row spacing of 0.3 nm give the **Ru2** island the striped appearance seen in Figure 2A. The **Ru2** rows are composed of **Ru2** molecules with their intramolecular metal−metal axes at a 30° angle to the main direction of the molecular row. Similar to the STM image of **Ru2** at lower coverage in Figure 1B, the two end groups within each **Ru2** molecule are indistinguishable in Figure 2A.

Received Date: October 28, 2009
Accepted Date: December 4, 2009
Published on Web Date: December 15, 2009

DOI: 10.1021/jz900197a | *J. Phys. Chem. Lett.* **2010**, *1*, 420–424

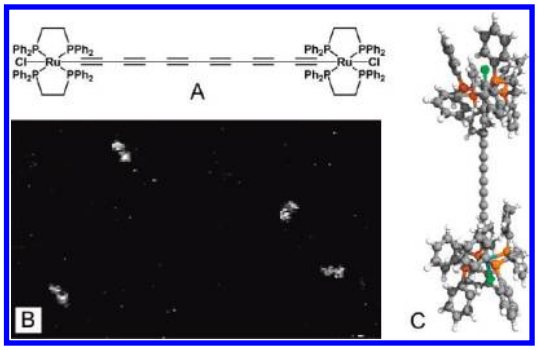

Figure 1. (A) Structural formula of **Ru2**; (B) isolated **Ru2** on Au(111), 0.5 V, 20 pA, 298 K, 400 Å × 250 Å; (C) ball-and-stick model of **Ru2**.

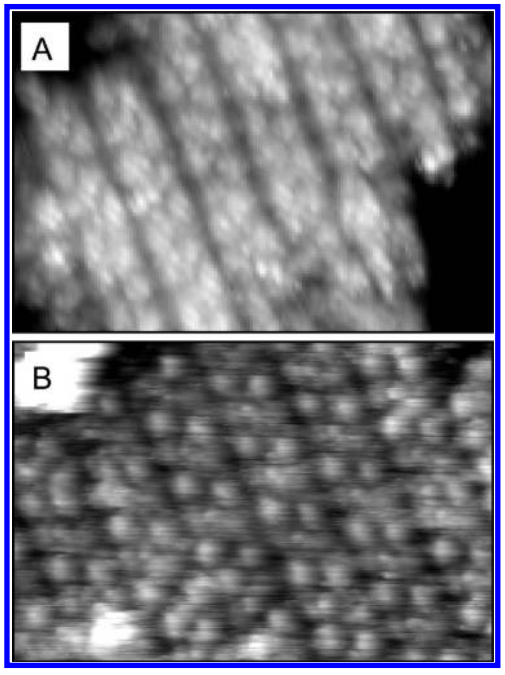

Figure 2. (A) 180 Å × 130 Å STM image of the **Ru2** monolayer on Au(111), 0.5 V, 20 pA, 77 K; (B) 180 Å × 130 Å STM image of the **Ru2**$^+$[PF_6]$^-$ monolayer on Au(111), 0.5 V, 20 pA, 77 K.

Figure 2B shows that at high coverage, **Ru2**$^+$[PF_6]$^-$ molecules form almost identical monolayer patterns on Au(111) at 77 K as **Ru2**; paired dots of **Ru2**$^+$ align together to form straight molecular rows spaced 0.3 nm apart, with each Ru−Ru intramolecular axis again angled 30° from the row direction.

While the two features of a **Ru2** molecule appear identical, the two features of a **Ru2**$^+$[PF_6]$^-$ molecule appear to have different contrast in STM images. In Figure 2B, the **Ru2**$^+$ monolayer has significant long-range superstructure, in which bright and dim stripes are formed with an angle of 60° from the **Ru2**$^+$ molecular row direction. We attribute this contrast difference to the uneven charge distribution between the two end groups of **Ru2**$^+$.

Figure 3A enlarges the monolayer area of Figure 2B to show a single molecular row in detail. With the boundary of the monolayer clearly visible in the STM image, the two features closest to the edge must belong to the same **Ru2**$^+$, and the rest of the **Ru2**$^+$ molecules within the chain can be assigned following this configuration. This model of the molecular row is shown in Figure 3B. The connection between electronic properties and imaging contrast in STM images is complex, and while we observe a strong contrast difference between the two end groups of each **Ru2**$^+$, it is difficult to conclude from this image alone which one is the charged end group in Figure 3A.

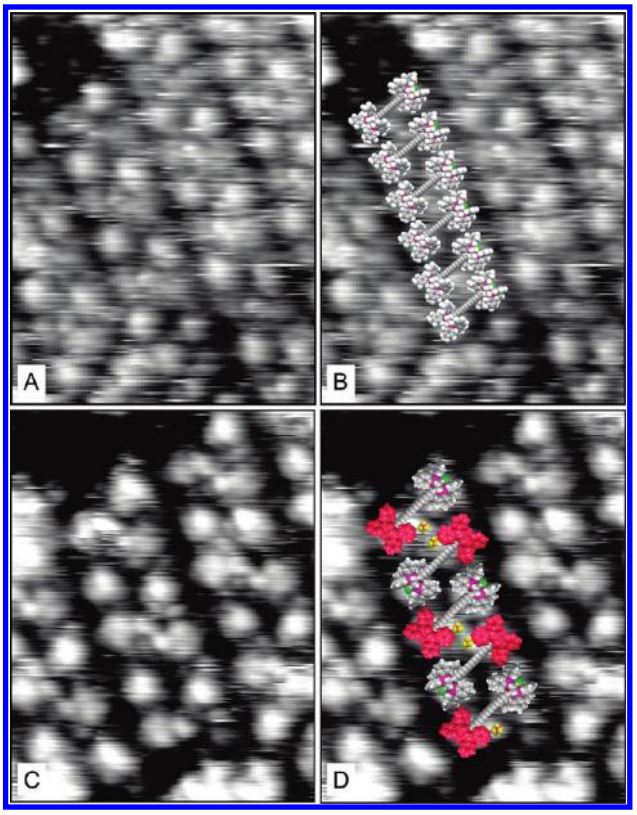

Figure 3. (A) 95 Å × 120 Å STM image of the **Ru2**$^+$[PF_6]$^-$ monolayer on Au(111), 0.5 V, 20 pA, 77 K; (B) same view as (A), with scaled ball-and-stick model of **Ru2**$^+$ molecules to show the position of each **Ru2**$^+$ within one molecular chain; (C) 75 Å × 100 Å STM image of the **Ru2**$^+$[PF_6]$^-$ monolayer on Au(111), −0.5 V, 20 pA, 77 K; (D) same view as (C), with scaled ball-and-stick model of **Ru2**$^+$ and [PF_6]$^-$ to show the position of each bf **Ru2**$^+$ and [PF_6]$^-$ within one molecular chain.

High-resolution STM images of a **Ru2**$^+$ monolayer on Au(111) are shown in Figure 3C. Again, the positions of each **Ru2**$^+$ within one molecular row can be assigned starting from the monolayer edge. As in Figure 2B, each **Ru2**$^+$ is composed of one brighter feature and one dimmer feature. This higher-resolution STM image shows small features scattered among the **Ru2**$^+$ on the surface, with sizes of 3−4 Å. During the pulse-deposition process, the **Ru2**$^+$[PF_6]$^-$ solution is deposited onto the Au(111) surface under vacuum, and the solution is composed of toluene molecules (6 Å × 4.3 Å), **Ru2**$^+$ cations (29 Å × 13 Å), [PF_6]$^-$ anions (3.2 Å × 3.2 Å), ferrocene molecules (4.2 Å × 3.5 Å), unreacted ferrocenium cations (4.2 Å × 3.5 Å), and unreacted **Ru2** molecules (29 Å × 13 Å). Of these, **Ru2**$^+$, **Ru2**, and toluene molecules are too large to

DOI: 10.1021/jz900197a | J. Phys. Chem. Lett. 2010, 1, 420–424

match the small features in Figure 3C; ferrocene molecules and ferrocenium ions are slightly too large; and $[PF_6]^-$ anions are a close match to the feature size. Further examination of Figure 3C shows that most of these additional small features appear next to the dimmer end groups of **Ru2**$^+$. The most plausible explanation is that these small features are $[PF_6]^-$ anions that associate with the positively charged end group of **Ru2**$^+$. Under this interpretation, the positively charged end group appears dimmer in STM images. Coulomb interactions will stabilize the positions of $[PF_6]^-$, and the presence of $[PF_6]^-$ next to one end group of **Ru2**$^+$ may help to localize the positive charge in the neighboring metal complex.

On the basis of these interpretations, we label every species within one molecular row in Figure 3C and show the resulting model in Figure 3D. The neutral end groups of **Ru2**$^+$ are shown in gray, while the positively charged end groups of **Ru2**$^+$ are colored red; the small yellow features represent the $[PF_6]^-$ counterions. Within each molecular line, the neighboring **Ru2**$^+$ molecules have opposite polarizations. This interlacing dipole packing demonstrates that the Coulomb interactions between neighboring **Ru2**$^+$ molecules are strong;[24] this is a necessary prerequisite for the transfer of binary information in QCA. The packing of the **Ru2**$^+$ molecular line is very similar to the QCA binary wire proposed in the original QCA concept,[25] with the main difference being the titling of the main axis of each **Ru2**$^+$. This tilting of the each **Ru2**$^+$ within the molecular row likely results from the hexagonal symmetry of the underlying Au(111) lattice, and switching to a surface with square or rectangular symmetry might lead to a better-aligned molecular pattern.

The model in Figure 3D places pairs of $[PF_6]^-$ anions in close proximity, with an observed $[PF_6]^-$–$[PF_6]^-$ distance of 6–7 Å. As both are negatively charged, this close spacing is initially counterintuitive. We understand this observation through comparison to the X-ray diffraction (XRD) measurements of Fehlner and co-workers, who determined the structure of single-crystal *trans*-$[(H_2NCH_2CH_2\ C{\equiv}N)(dppe)_2Ru(C{\equiv}C)_6Ru(dppe)_2\ (N{\equiv}CCH_2CH_2NH_2)]\ [PF_6]_2$ (dppe = diphenylphosphinoethane), a derivative of **Ru2**.[18] This diruthenium complex shares the same overall Ru–Ru structure of **Ru2** but has both of the Ru-centered end groups positively charged. Pairs of closely spaced $[PF_6]^-$ anions are also observed in the XRD structure, with a $[PF_6]^-$–$[PF_6]^-$ distance of 7.7 Å, a distance that is similar to the 6–7 Å that we measured. We note that STM topography shows only a two-dimensional projection of a three-dimensional distance, and slightly reduced distances are expected if structures are nonplanar. In any case, given the comparison between related but not identical molecules, this is a high level of qualitative agreement. The XRD structure also shows that each $[PF_6]^-$ anion is located near a ruthenium center but is displaced slightly inward along the Ru–Ru bond toward the opposite ruthenium. This behavior is similar to that observed in our STM images of **Ru2**$^+[PF_6]^-$, as shown in Figure 3D. We again observe a reduced distance, 9.5 Å between the closest Ru metal center and $[PF_6]^-$ in the XRD structure, compared to 6 Å in our STM measurements. These similarities further support the model presented in Figure 3D.

STM images show a combination of topographic and electronic features of the surface, and the electronic effects

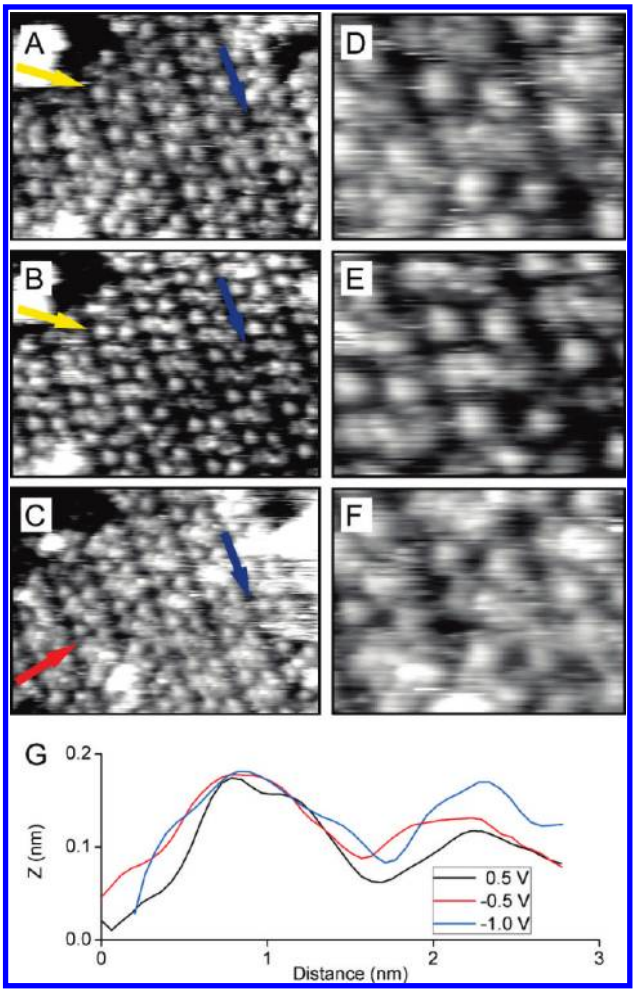

Figure 4. Left column: 180 Å × 130 Å STM image of the **Ru2**$^+$-$[PF_6]^-$ monolayer on Au(111) under various bias voltages. (A) 0.5 V, 20 pA, 77 K; (B) −0.5 V, 20 pA, 77 K; (C) −1.0 V, 20 pA, 77 K. Right column: enlarged area from corresponding images in the left column; size: 75 Å × 55 Å. (G) Height profiles of one **Ru2**$^+$ at various bias voltages.

can potentially be deconvoluted from physical topography through the use of scanning tunneling spectroscopy and bias-dependent imaging. Figure 4A–C shows STM images of the same area of a **Ru2**$^+[PF_6]^-$ monolayer on Au(111) at various tip–sample bias voltages, with the differences between these three STM images arising from the spatial dependence of the local density of electronic states. The primary characteristic of the **Ru2**$^+[PF_6]^-$ monolayer on Au(111), visible in all three STM images, is the parallel, straight molecular rows. These molecular rows define the direction **MC** (molecular chain), marked with the blue arrows in Figure 4A–C. When the sample is positively biased as in Figure 4A, the STM image shows the empty states of the adsorbates on the surface.[26] The secondary structure is the interlaced stripes of bright and dim features within the monolayer along direction **NC** (neutral and charged), marked with the yellow arrows in Figure 4A and B. The direction **NC** has an angle of 58° with respect to the direction **MC**. When the sample is negatively biased, the STM image shows the filled states of the adsorbates on the surface,

DOI: 10.1021/jz900197a | J. Phys. Chem. Lett. 2010, 1, 420–424

as shown in Figure 4B and C. The third visible superstructure is along the direction **DM** (double molecules), marked with a red arrow in Figure 4C. The angle between direction **DM** and **MC** is 78°. This superstructure is only visible when the tip−sample bias voltage is −1.0 V. Along the directions **DM** and **MC**, the **Ru2**$^+$[PF_6]$^-$ monolayer can be described by a unit cell composed of two complete **Ru2**$^+$ cations.

The right column of Figure 4 shows magnified views of each corresponding STM image in the left column; the same area of the surface is shown in each magnified image. Although the STM images acquired at 0.5 and −0.5 V are very similar to each other, the charged end groups of **Ru2**$^+$ appear dimmer at 0.5 V than at −0.5 V, while the contrast of the neutral features is almost constant. When the sample is biased at −1.0 V, the charged end groups of **Ru2**$^+$ have similar STM contrast as the neutral end groups, which is shown in Figure 4F. This suggests that the charged end groups, along with the [PF_6]$^-$ counterions next to them, have an electronic density of states that changes more with energy than that of the neutral end groups. This trend is clearly shown in the cross-sectional height profiles of these three scanning biases in Figure 4G. Because of the limited resolution in Figure 4, we cannot assign which is more responsible for the contrast change, the charged end groups of **Ru2**$^+$ cations or their [PF_6]$^-$ counterions.

In conclusion, a dinuclear organometallic complex is singly oxidized in solution, and the adsorption of the oxidized mixed-valence species on Au(111) is observed at submolecular resolution by low-temperature STM. The different contrast between the two end groups of **Ru2**$^+$ in STM images is attributed to the extra charge localized on one of the end groups of **Ru2**$^+$. The counterions show very strong interactions with mixed-valence cations by retaining their proxmity to the cations on the surface. The mixed-valence dinuclear complex form straight molecular lines by alternating polarization of neighboring molecules. The observed molecular line is very similar to the QCA configuration suggested in the QCA proposal.[25]

EXPERIMENTAL METHODS

Ru2 was synthesized by following procedures set out by Chaudret et al.[27] and Rigaut et al.[28] A nitrogen-purged drybox was used to prepare a solution of 0.5 mg of **Ru2** in 5 mL of toluene to avoid possible degradation due to air and water sensitivity of **Ru2**. **Ru2** on Au(111) samples were prepared by the pulse-injection technique discussed in previous publications.[22,23,29,30]

The mixed-valence complex **Ru2**$^+$[PF_6]$^-$ was made by mixing **Ru2** with ferrocenium hexafluorophosphate ([Fe(η^5-C_5H_5)$_2$][PF_6]) in a 1:1 mol ratio in toluene solution in a nitrogen-purged drybox

$$\mathbf{Ru2} + [\mathrm{Fe}(\eta^5 - \mathrm{C_5H_5})_2][\mathrm{PF_6}] \xrightarrow{\text{toluene}} [\mathbf{Ru2}]^+[\mathrm{PF_6}]^- + \mathrm{Fe}(\eta^5 - \mathrm{C_5H_5})_2$$

After the oxidation reaction, the **Ru2**$^+$[PF_6]$^-$ solution was pulse-deposited without further purification onto Au(111) under vacuum to make **Ru2**$^+$[PF_6]$^-$ on Au(111). Samples were imaged at room and low temperatures using a UHV STM (Omicron Nanotechnology LT-STM) in constant-current mode using mechanically cut Pt−Ir tips.

AUTHOR INFORMATION

Corresponding Author:

*To whom correspondence should be addressed. E-mail: skandel@nd.edu.

Present Addresses:

†Department of Chemistry and Biochemistry, Center for Nano- and Molecular Science and Technology, the University of Texas at Austin, Austin, Texas 78712.

ACKNOWLEDGMENT This work was supported by NSF NIRT Grant #0403760. The authors acknowledge Dr. Roger Nassar and Prof. Thomas P. Fehlner, who synthesized the **Ru2** molecules used in this study.

REFERENCES

(1) Avouris, P. Molecular Electronics with Carbon Nanotubes. *Acc. Chem. Res.* **2002,** *35*, 1026–1034.
(2) Nitzan, A. Electron Transmission through Molecules and Molecular Interfaces. *Annu. Rev. Phys. Chem.* **2001,** *52*, 681–750.
(3) Joachim, C.; Gimzewski, J. K.; Aviram, A. Electronics Using Hybrid-Molecular and Mono Molecular Devices. *Nature* **2000,** *408*, 541–548.
(4) Tour, J. M. Molecular Electronics. Synthesis and Testing of Components. *Acc. Chem. Res.* **2000,** *33*, 791–804.
(5) Blum, A.; Kushmerick, J.; Long, D.; Patterson, C.; Yang, J.; Henderson, J.; Yao, Y.; Tour, J.; Shashidhar, R.; Ratna, B. Molecularly Inherent Voltage-Controlled Conductance Switching. *Nat. Mater.* **2005,** *4*, 167–172.
(6) Barth, J. V.; Costantini, G.; Kern, K. Engineering Atomic and Molecular Nanostructures at Surfaces. *Nature* **2005,** *437*, 671–679.
(7) Javey, A.; Kim, H.; Brink, M.; Wang, Q.; Ural, A.; Guo, J.; McIntyre, P.; McEuen, P.; Lundstrom, M.; Dai, H. High-Kappa Dielectrics for Advanced Carbon-Nanotube Transistors and Logic Gates. *Nat. Mater.* **2002,** *1*, 241–246.
(8) Vogel, E. M. Technology and Metrology of New Electronic Materials and Devices. *Nat. Nanotechnol.* **2007,** *2*, 25–32.
(9) Haider, M. B.; Pitters, J. L.; DiLabio, G. A.; Livadaru, L.; Mutus, J. Y.; Wolkow, R. A. Controlled Coupling and Occupation of Silicon Atomic Quantum Dots at Room Temperature. *Phys. Rev. Lett.* **2009,** *102*, 046805.
(10) Kim, S. B.; Pike, R. D.; D'Acchioli, J. S.; Walder, B. J.; Carpenter, G. B.; Sweigart, D. A. Patterned Monolayers of Neutral and Charged Functionalized Manganese Arene Complexes on a Highly Ordered Pyrolytic Graphite Surface. *Angew. Chem., Int. Ed.* **2009,** *48*, 1762–1765.
(11) Kirczenow, G.; Piva, P. G.; Wolkow, R. A. Modulation of Electrical Conduction through Individual Molecules on Silicon by the Electrostatic Fields of Nearby Polar Molecules: Theory and Experiment. *Phys. Rev. B* **2009,** *80*, 035309.
(12) Lin, N.; Stepanow, S.; Ruben, M.; Barth, J. V. Surface-Confined Supramolecular Coordination Chemistry. *Top. Curr. Chem.* **2009,** *287*, 1–44.
(13) Lent, C. S.; Tougaw, P. D.; Porod, W. Bistable Saturation in Coupled Quantum Dots for Quantum Cellular Automata. *Appl. Phys. Lett.* **1993,** *62*, 714–716.

DOI: 10.1021/jz900197a | *J. Phys. Chem. Lett.* **2010,** *1*, 420–424

(14) Orlov, A. O.; Amlani, I.; Bernstein, G. H.; Lent, C. S.; Snider, G. L. Realization of a Functional Cell for Quantum-Dot Cellular Automata. *Science* **1997,** *277*, 928–930.
(15) Cole, T.; Lusth, J. C. Quantum-Dot Cellular Automata. *Prog. Quantum Electron.* **2001,** *25*, 165–189.
(16) Manimaran, M.; Snider, G. L.; Lent, C. S.; Sarveswaran, V.; Lieberman, M.; Li, Z. H.; Fehlner, T. P. Scanning Tunneling Microscopy and Spectroscopy Investigations of QCA Molecules. *Ultramicroscopy* **2003,** *97*, 55–63.
(17) Tokunaga, K. Signal Transmission through Molecular Quantum-Dot Cellular Automata: A Theoretical Study on Creutz-Taube Complexes for Molecular Computing. *Phys. Chem. Chem. Phys.* **2009,** *11*, 1474–1483.
(18) Qi, H.; Gupta, A.; Noll, B. C.; Snider, G. L.; Lu, Y. H.; Lent, C.; Fehlner, T. P. Dependence of Field Switched Ordered Arrays of Dinuclear Mixed-Valence Complexes on the Distance between the Redox Centers and the Size of the Counterions. *J. Am. Chem. Soc.* **2005,** *127*, 15218−15227.
(19) Qi, H.; Sharma, S.; Li, Z. H.; Snider, G. L.; Orlov, A. O.; Lent, C. S.; Fehlner, T. P. Molecular Quantum Cellular Automata Cells. Electric Field Driven Switching of a Silicon Surface Bound Array of Vertically Oriented Two-Dot Molecular Quantum Cellular Automata. *J. Am. Chem. Soc.* **2003,** *125*, 15250–15259.
(20) Goeltz, J. C.; Kubiak, C. P. Mixed Valence Self-Assembled Monolayers: Electrostatic Polarizabilities of the Mixed Valence States. *J. Phys. Chem. C* **2008,** *112*, 8114–8116.
(21) Lu, Y.; Lent, C. S. Theoretical Study of Molecular Quantum-Dot Cellular Automata. *J. Comput. Electron.* **2005,** *4*, 115–118.
(22) Wei, Z. Q.; Guo, S.; Kandel, S. A. Observation of Single Dinuclear Metal-Complex Molecules Using Scanning Tunneling Microscopy. *J. Phys. Chem. B* **2006,** *110*, 21846–21849.
(23) Guo, S.; Kandel, S. A. Scanning Tunneling Microscopy Studies of Pulse Deposition of Dinuclear Organometallic Molecules on Au(111). *J. Chem. Phys.* **2008,** *128*, 014702.
(24) Baber, A. E.; Jensen, S. C.; Sykes, E. C. H. Dipole-Driven Ferroelectric Assembly of Styrene on Au(111). *J. Am. Chem. Soc.* **2007,** *129*, 6368–6369.
(25) Lent, C. S.; Isaksen, B.; Lieberman, M. Molecular Quantum-Dot Cellular Automata. *J. Am. Chem. Soc.* **2003,** *125*, 1056–1063.
(26) Hamers, R. J. Scanned Probe Microscopies in Chemistry. *J. Phys. Chem.* **1996,** *100*, 13103–13120.
(27) Chaudret, B.; Commenges, G.; Poilblanc, R. Bis(diphenylphosphino)methane Complexes of Ruthenium(0) and Ruthenium(II). *J. Chem. Soc., Dalton Trans.* **1984,** 1635–1639.
(28) Rigaut, S.; Perruchon, J.; Le Pichon, L.; Touchard, D.; Dixneuf, P. H. Synthesis of Ruthenium Acetylides: New Building Blocks for Molecular Electronics. *J. Organomet. Chem.* **2003,** *670*, 37–44.
(29) Leon, C. P.; Surgers, C.; Mayor, M.; Marz, M.; Hoffmann, R.; von Lohneysen, H. STM Investigation of Large p-Conjugated Oligomers and Tetrahydrofuran Codeposited on Cu(111) by Pulse Injection. *J. Phys. Chem. C* **2009,** *113*, 14335−14340.
(30) Tanaka, H.; Hamai, C.; Kanno, T.; Kawai, T. High-Resolution Scanning Tunneling Microscopy Imaging of DNA Molecules on Cu(111) Surfaces. *Surf. Sci.* **1999,** *432*, L611–L616.

DOI: 10.1021/jz900197a | *J. Phys. Chem. Lett.* **2010,** *1*, 420–424